JOINT EUROPEAN TORUS

JET–P(91)44

V.P. Bhatnagar, J. Jacquinot, C. Gormezano, D.F.H. Start
and JET Team

ICRF Heating and Synergistic LH and Fast-Wave Current Drive in JET

ICRF Heating and Synergistic LH and Fast-Wave Current Drive in JET

V.P. Bhatnagar, J. Jacquinot, C. Gormezano, D.F.H. Start
and JET Team*

JET-Joint Undertaking, Culham Science Centre, OX14 3DB, Abingdon, UK

** See Appendix 1*

Preprint of an Invited Paper presented to 9th Topical Conference on
Radio Frequency Power in Plasmas, Charleston, USA., 19th-21st August 1991

Invited Paper for the Ninth Topical Conference on Radio Frequency Power in Plasmas, Charleston, U.S.A., 19-21 August 1991.

ICRF HEATING AND SYNERGISTIC LH AND FAST-WAVE CURRENT DRIVE IN JET

V.P. Bhatnagar, J. Jacquinot, C. Gormezano, D.F.H. Start and the JET Team
JET Joint Undertaking, Abingdon, OXON, OX14 3EA (U.K.)

ABSTRACT

Ion cyclotron resonance heating (ICRH) experiments in JET have been carried out in a variety of scenarios using advanced antennas, phasing and matching techniques leading to improved plasma performances. A record ICRH power of 22 MW has been coupled to the plasma in L-mode with $\tau_E \cong 1.3\tau_G$ where τ_G refers to the Goldston L-mode prediction for the energy confiment time. Also, $\cong 3MW$ has been coupled for as long as 1 minute with little change in Z_{eff}. ICRH produced H-modes have $\tau_E \cong 2.8\tau_G$ with a duration of 2.8 s at power levels of $\lesssim$ 12 MW. Pellet produced peaked-density profile reheated with ICRH have been combined with H-modes to produce $T_{i0} \geq T_{e0}$ and highest thermonuclear yield where the **thermal** triple fusion product $n_D(0) \cdot \tau_E \cdot T_i(0) \cong 7.8 \cdot 10^{20}\ m^{-3}skeV$ has been achieved. Good confinement and ion heating ($T_{i0} \geq T_{e0}$) have been demonstrated both in the two-minority scheme as well as in the high-minority heating scenario (H-minority in He3-plasmas) where $n_H/n_e \lesssim 0.4$ was reached. Unidirectional superthermal electrons ($\cong 100 - 200keV$) produced by lower-hybrid current drive (LHCD) system have been synergistically accelerated by transit-time magnetic pumping (TTMP) of fast-waves coupled by ICRH in the (0,0)-phasing of the antenna. This produces TTMP current drive even without phasing the ICRH antennas. Finally, in the minority current-drive scenario which is predicted to control the shear (dq/dr), marked differences in the sawteeth behaviour have been observed in experiments when the phase of the antennas was reversed while depositing power near the q = 1 surface.

1. INTRODUCTION

1.1 ICRH Antenna System: The ICRH system of JET [1,2] consists of a total generator power of 32 MW, 20 s, 25-55 MHz and uses eight antennas that are distributed symmetrically around the torus. A JET antenna has two radiating elements that are separated toroidally which can be phased arbitrarily but are generally driven in (0,0)-phasing (monopole) or (0, π)-phasing (dipole). The antenna screens are made of one tier of beryllium rods [3] which are inclined at 15° (from the toroidal direction) to align them approximately with the total field. The screens also feature a symmetric shallow V design to avoid extraneous contact with the plasma due to the toroidal field ripple and in the dipole phasing, it permits an antisymmetry of lines of force touching on the two sides of the antenna. The choice of Be (which has low sputtering coefficient at high energy 0.2 to 0.6 kV) has eliminated the impurity release from sputtering by (Be, C, O) ions accelerated in the electric field produced by the sheath rectification of the applied RF voltage. Thus ICRH specific impurities have been reduced to negligible levels in all conditions of ICRH operation in JET.

1.2 ICRH Matching and Phasing System: In the JET ICRH system, an automatic generator-antenna matching [4] is achieved by feedback on two quasi-independent parameters, namely the frequency of the generator (response time τ = 1 ms) and the stub-length (τ = 0.3-0.5 s). However, during an L to H-mode transition there is a steepening of the edge-density profile which leads to a sudden decrease of the coupling resistance. Matching under such conditions is facilitated by implementing a radial plasma position feedback control (τ = 30 ms) by acting on the current of the vertical field winding. This maintains the coupling resistance constant

at a desired value. In this case, frequency feedback with only minor movement of stubs attains the match. The generator frequency feedback control is necessary to compensate for the changes in the reactive part of the loading during an L-H transition. Thus three feedback loops (frequency, stub length and plasma position) have allowed the matching to be maintained satisfactorily during an L-H transition even with a three-fold steepening of the edge density gradient.

The above versatile automatic VSWR control system [4] has also permitted the matching of a coupled pair of straps in an antenna with arbitrary phasing [5] when the $|I|$ in both straps is maintained equal. Starting from a (0,0)-phasing match of a plasma with a loading resistance of $\cong 4\Omega$, in the first shot, the phase is linearly increased to (+45,-45) in about 6 s with stubs, trombones (line-lengths) and frequency under automatic real-time tracking for a match. In the next shot, (+45,-45)-phasing is fixed and a desired power is driven under phased condition. The RF power output, though not fully regulated in this mode of operation, is reasonably constant. This operation has worked well and $\cong 5MW$ has been coupled using 4 antennas under minority ion current drive scenario.

2. ICRH L-MODE.

ICRH power upto 22 MW has been coupled to a Be belt-limiter plasma in the JET tokamak [6] at an $I_P = 3MA$ and $B_\phi = 2.8T$. Typical time traces of such a discharge are shown in Fig.1 where the (H)-minority in D-plasma was heated with dipole phasing. The diamagnetic stored energy $W_{DIA} \cong 1.4 \cdot W_G$ where W_G is the Goldston [7] L-mode prediction. The plasma density was high and the enrgy stored in the fast-ions was about 15%. In these discharges, the power depostion was central which lead to monster sawteeth (period greater than the energy confinement time) and central electron temperature (T_{e0}) was roughly 1.6 times higher than the central ion temperature (T_{i0}). The radiated power was $P_{rad}/P_{tot} \cong 0.1$ to 0.25 and Z_{eff} in these discharges ranged between 1.4 to 2.3.

In Fig. 2, we present time traces of a 2 MA (magnetically) steady-state discharge in JET of a duration of $\cong$60 s which was heated by ICRH at a level of $\cong 3MW$ for the entire duration of the discharge by energizing 2 to 3 antennas successively from the available 8 units. Z_{eff} remained low (≤ 1.3) for the entire duration of the pulse. Particle recyling was not in steady state. By electron heating, the ICRH extended the pulse lenth by 16 s. In another discharge, the pulse length could be extended even further by electron heating due to ICRH and assisted current drive by LHCD system.

3. ICRH H-MODE.

3.1 Plasma Configuration: For ICRH H-mode discharges, a double-null X-point configuration is chosen (see Fig. 3) as the power loading on the target tiles is shared as compared to a single null discharge. Also, in this case the last closed flux surface can be shaped poloidally to match the antenna profile to obtain a good antenna plasma coupling.

3.2 Typical Time Traces: Typical time traces of an ICRH H-mode obtained with dipole are shown in Fig. 4 from where one can see all characteristics typical of H-mode discharges such as a drop in D_α emission, increase in plasma density, an increase in stored energy at the transition (at constant power level) and an increase in the DD-reaction rate etc. In this shot the energy confinement time $\tau_E \cong 2.8\tau_G$ where τ_G refers to the Goldston [7] L-mode prediction. The DD reaction rate (R_{DD}) of $5.5 \cdot 10^{15}$ /s achieved is about a factor of 10 higher than the value obtained at the same power level in 3 MA limiter discharges. Note that the discharge is ELM free. In another discharge, the duration of an ICRH H-mode of about 2.8 s has been achieved.

3.3 Global Energy Confinement: A plot of stored energy W (from diamagnetic-loop measurement) plotted as a function of P_T-dW/dt for ICRH H-mode discharges at $I_p = 3.1$ MA using dipole and monopole phasing is shown in Fig. 5. The lines drawn on the figure represent a multiple of the Goldston [7] L-mode prediction W_G for deuterium discharges. For discharges with dipole $1.8 < W/W_G < 2.8$ whereas with monopole $W/W_G \cong 1.7$ for a loss power of about 8 MW.

3.4 Comparison of Monopole and Dipole Phasing: ICRH H-modes are generally accompanied by monster sawtooth especially with monopole phasing. At 2.8 T, the power threshold for transition to an H-mode with monopole is about 8 MW whereas it is about 5 MW with dipole. Also, the steepening of edge density profile with monopole is smaller than that with dipole. The above poorer performance of H-modes with monopole is not associated with higher impurity influx as with beryllium antenna screen, the behaviour of radiated power from low and high-Z impurities in an H-mode produced with monopole is similar to that found in dipole [8]. Based on the RF sheath rectification theory [9,10] it can be argued that monopole produces some modification of the plasma edge through the formation of a convective cell [9] due to the ExB drift (electric field produced by sheath rectification of the RF voltage) in the poloidal direction which reduces as one moves away from the antenna. The length of the cell is about the size of the screen in the poloidal direction, it has a width of about 4 cm and can penetrate to a depth of about 2 cm into the plasma [9]. The formation of the cell is inhibited in the dipole phasing due to electric field being zero on the average whereas in monopole it can be eliminated only when the screen bars are fully aligned with the total magnetic field.

4. PELLET ENHANCED PERFORMANCE COMBINED WITH H-MODE

In 1988-89, deep pellet-fueled peaked-density profiles ($n_{e0}/\langle n_e \rangle \cong 3$) produced in non-sawtoothing limiter plasmas of JET were reheated with high power ($\approx$12 MW) minority ICRF heating [11,12]. These peaked profiles with a maximum $n_{e0} = 1.4 \cdot 10^{20} m^{-3}$ were sustained for up to 1.2 s and lead to an improvement in the core confinement resulting in high values of central electron and ion temperatures simultaneously with an increased nuclear reactivity of the plasma. This improved phase was termed as Pellet Enhanced Phase (PEP). In 1990-91, the improved core confinement of the PEP phase was combined with the improved edge confinement of the H-mode in a double-null X-point plasma giving PEP+H phase [9,13]. This phase provides the highest thermo-nuclear yield at high density with $T_{e0} \cong T_{i0}$ as compared to some other hot-ion regimes where the target density is necessarily low. Typical time traces of such a discharge are shown in Fig. 6 where a 4 mm pellet (speed $\cong$ 2.5 km/s) is injected at the begining of the current plateau. ICRH power ramp and the diagnostic neutral beam injection (140 keV) is made to coincide with the pellet injection. This produces a peaked density profile ($n_{e0}/\langle ne \rangle \cong 3.5$) leading to the PEP mode. The peaked profile decays slowly and after about a second, an H-transition is triggered as evidenced by the D_α trace and the stored energy continues to rise. PEP+H phase often lasts $\cong$0.5 s and becomes an ordinary H-mode after a series of MHD events [14]. Generally, there is a crash in the DD-reaction rate (due to MHD activity) but in this shot it gently rolls over. The H-phase in this case lasts practically until the end of the heating pulse. The T_{e0} and T_{i0} both attained 10 keV at $n_{e0} \cong 4 \cdot 10^{19} m^{-3}$. The radiated power remains at a level of 2 MW through the heating phase. In another shot where the ICRH power was delayed by 0.5 s after the pellet, T_{e0} and T_{i0} both achieved 15 keV simultaneously at a slightly lower n_{e0} but practically at the same total input power. Several such variations were made to optimise the performance. In a shot, $T_{i0} \cong 16.5 keV$ and $T_{e0} \cong 14.5 keV$ were obtained. In these discharges, the neutron yield is about 5 times the ordinary ICRH H-modes and twice as high as the PEP modes [9,13]. Neutron spectroscopy indicates that

about 80% of the neutrons are thermal. The global confinement time is generally about the same or slightly better than the ICRH H-modes [9,13,15].

Local transport analysis [26] of such discharges using FALCON and TRANSP codes shows that effective heat conduction coefficient $\chi_{eff} \cong 0.5m^2/s$ in the core region ($r < 0.4$ a) which is about a factor 2 lower than the normal H-mode value. Outside the core region, $\chi_{eff} \cong 1 - 2m^2/s$ which is similar to that of normal H-modes. The reason for the enhanced central confinement is not yet fully understood but there is a strong indication from MHD studies [14] that the central q-profile is flat or hollow which could stabilise ballooning modes. It is believed that initially this shear inversion is produced by the pellet injection and it is then sustained or even increased by the bootstrap current. If this interpretation is correct, this enhanced mode which occurs only transiently, could be sustained by current profile modification by non inductive means such as minority current drive (see below) or a combination of TTMP and LHCD.

5. HIGH-MINORITY ICRF HEATING EXPERIMENTS

In the active phase of JET and, to ease ignition in a reactor, it has been proposed to use ICRH with high concentration D-minority heating in a tritium plasma [16]. The aim is to reduce the minority tail energy such that it is optimum for the D-T fusion cross section. This will produce significant levels of ICRF-driven D-T fusion reactivity [17]. Also, it will allow dominant background ion-heating from the minority as its tail would be below the critical energy. In a reactor, from penetration considerations, NBI is planned at MeV range of energies which will lead to electron heating. But, transport calculations show that the most power-efficient route to ignition in a reactor will be via the heating of ions. Calculations for NET/ITER show that in the minority heating, for $n_D/n_T = 30\%$, at least 50% of the power will go to ions [18].

In the ICRF heating, as the minority ion concentration is increased, minority heating changes to mode conversion. When the antenna is located on the low-field-side, a further increase leads to the occurence of radial eigenmodes. Mode conversion can be avoided if the following condition is satisfied:

$$\frac{n_{\min}}{n_{maj}} \lesssim 2 \cdot \frac{k_{\parallel} v_{\parallel}}{\omega} \left[\frac{Z_{maj}^2 M_{\min}}{Z_{\min}^2 M_{maj}} \right] \left\{ \frac{1}{1 - \left(\frac{Z_{maj}/M_{maj}}{Z_{\min}/M_{\min}} \right)^2} + \frac{k_{\parallel}^2 c^2}{\omega_{pmaj}^2} \right\}$$

where $v_{\parallel}$ is the velocity obtained from the minority ion parallel temperature and other symbols have their usual meaning. Thus higher minority concentration can be tolerated if higher $k_{\parallel}$ or (0, π)-phasing is used, higher $v_{\parallel}$ is used (or as the minority heats up) and appropriate minority/majority species are selected. Hydrogen minority in He3 majority plasma offers best combination as seen in Fig. 7. Typical time traces of a H-minority ICRF heating in 3 MA He3 limiter plasma at about 10 MW of RF power are shown in Fig. 8 where n_h/n_e was about 30%. The experiment was done at a higher density ($n_{e0} \cong 5 \cdot 10^{19} m^{-3}$) to reduce the tail further. The tail temperature as measured by a neutral particle analyser (NPA) plotted as a function of n_H/n_e is shown in Fig. 9. The tail temperature decreased with increasing H-concentration and was near the critical energy. At a given $P_{tot}/n_{e0} \cong 2.3 \cdot 10^{-19} MW/m^{-3}$, it is found that T_{i0} is higher and T_{e0} lower by about 30% when compared with (H)-D discharges at lower minority (5%) concentration. The global energy confinement was similar to other L-mode ICRH discharges with $\tau_E \cong 1.3\tau_G$. The minority concentration was determined by the density-rise method when hydrogen was puffed. The concentration

thus obtained were found to be consistent with a calculation based on Stix model [19] using the measured fast-ion energy and the NPA measured tail temperature. We point out that majority ion heating has also been achieved in PEP+H modes with $n_H/n_e \cong 15\%$ in (H)-D plasmas [20].

It has been found that using high power low concentration H-minority heating in D-plasma, the electron heating is dominant (see Fig. 1) as the strong minority tail produced relaxes on electrons. To achieve ion heating, the minority tail energy has to be lower or close to the critical energy [19]. This can be achieved by using two minorities (H and He3) in D-plasmas and couple half the power in each species at two appropriate but different frequencies so that minority tail is shorter for each and relaxes more on ions. Moreover, He3-minority (though a weak damping scenario) is especially suitable for ion heating due to its charge and mass as it produces shorter tails and its critical energy is 3 times higher than hydrogen. Time traces of such a discharge with $B_\phi = 3.2T$ and $I_P = 3MA$ are shown in Fig. 10. where 9 MW was tuned to H-minority at 48 MHz and 6.6 MW to He3-minority at 32 MHz. In the absence of any other reliable minority concentration diagnostics, $n_{He3}/(n_H + n_D) \cong 0.085$ and $n_H/(n_{He3} + n_D) \cong 0.12$ were estimated based on the quantity of gas fed in the shot and it does not take the recycling into account. As in the high minority heating, $T_{i0} \geq T_{e0}$ (see Fig. 10) which represents an enhancement of T_{i0} and a reduction of T_{e0} in comparison with low H-minority case in Fig. 1. The T_{i0} is measured by Doppler broadening of Ni^{27}-line . When the corrections for burn out of this line in the center and profile effects are made, typically 30% higher values are found which are in agreement with charge exchange recombination spectroscopy. The values of T_{i0} quoted here are therefore an underestimate. This scenario was unfavourable to producing monster sawtooth. DD reaction rate was lower and radiated power higher in this shot due to an increase in Z_{eff} as the plasma touched the antenna due to a higher than usual triangularity.

6. SYNERGISTIC LOWER-HYBRID AND FAST-WAVE CURRENT DRIVE

A prototype lower-hybrid current drive (LHCD) launcher [21] fed by 8 klystrons at 3.7 GHz has coupled about 2 MW to JET plasmas with $n_\parallel \cong 2$ resonating with electrons of parallel energy $\cong$ 100 keV via electron Landau damping. [22]. Localization of fast electrons has been observed using a Fast Electron Bremsstrahlung (FEB) camera [23]. The monopole (0,0 phasing) spectrum of a JET ICRH antenna extends from $-4 < n_\parallel < 4$ and thus it overlaps the LHCD spectrum. Though ICRH on its own may not be able to produce fast electrons due to the 'gap' problem (which may or may not exist !) but it can accelerate (synergistically) unidirectional fast electrons (100 keV or higher) produced by LHCD thus increasing the current drive efficiency of LHCD without having to phase the ICRH antennas. Lower-Hybrid is limited by the accesibility problem and can not go below a certain $n_\parallel$ for a given density, but ICRH can go down unhindered in $n_\parallel$ and continuously increase the energy of the fast electrons eventually going into MeV range where the current drive efficiency is high.

When lower hybrid and ICRH power (monopole) were applied to a limiter plasma, FEB camera showed the evidence of an increased 'photon temperature' [9,22] from that obtained by LHCD. The increase was higher off axis ($\cong$0.4 m) where the LH deposits its power and the population of fast electrons is highest. The fast electrons diffuse away and a small increase of photon temperature was also found on axis (see Fig. 11). This synergistic effect was also found on the T_{e0} [9] which was higher and more peaked for a given P_{tot}/n_{e0} with the combination of LHCD and ICRH (see Fig.12).

7. SAWTEETH UNDER MINORITY-ION CURRENT-DRIVE SCENARIO.

Minority ion current drive physics was first discussed by Fisch in 1981. Since then further investigation by several other authors have predicted rather low overall current drive efficiency. The resonant condition $\omega - \omega_{ci} = k_{\|} \bullet v_{\|i}$ suggests that the sign of the driven current reverses on the two sides of the minority cyclotron layer in a tokamak when the damping is not too strong. Since the effect is local, it can be used to advantage to modify the gradient of the plasma current density especially near the q = 1 surface either to stablise the sawteeth or vice versa [24]. However, the launched spectrum of the antenna has to be asymmetric to cause this effect. This can be achieved by phasing the antenna different from (0,0) or (0, π). In Fig. 13, we illustrate the radiated power spectrum of two-straps of a JET A1-antenna separated by 0.31 m when phased (0, $\pi/2$). For comparison we also include the symmetric spectrum of monopole and dipole phasings. In this calculation the effect of plasma on the fast-wave propagation has been fully taken into account. Note that the spectrum is asymmetric for (0, $\pi/2$) phasing with a directivity of 0.66 which in this case is maximum for this phasing.

An experiment with such a phasing in JET with (H)-D plasma at $B_\phi = 2.5T$ and $I_P = 2MA$ with a f = 42 MHz which locates cyclotron layer $R_{CH} \cong 2.7m$ whereas the q = 1 surface on the high field side was at $\cong$ 2.8m. As shown in Fig. 14, the effect of about 3-4 MW of +90° phased power was to increase the period and amplitude of sawteeth (monster-like behaviour) and the T_e-profile was peaked despite the off-axis heating. But, -90° phasing of the two straps made the sawteeth very frequent and very small in amplitude and the temperature profile was very flat. Large effects are seen with powers as low as 1.5 MW. Note also the behaviour of sawteeth during roughly the same amount of minority heating power in dipole phasing and during the ohmic phase. This effect will systematically be studied further to evaluate if the shear modification is really taking place and if so, how it can be used to advantage, for example, for confinement improvement, MHD physics studies etc.

8. DISCUSSION AND CONCLUSIONS.

In other studies such as in the advanced fuel $D-{}^3He$ ICRH experiments on JET, a record real fusion power of 140 kW (a reaction rate of $4.6 \bullet 10^{16}/s$) was obtained using 14 MW of ICRH power in the ^3He minority scheme in L-mode [9,25]. The fusion reactions were monitored by measuring the flux of 16.6 MeV γ-ray photons from d $[{}^3He, \gamma]{}^5$Li reactions. A direct correlation between the generated fusion power and the energy stored in the fast ^{3}He ions is observed which is found to be consistent with Stix model and can be simply written as $P_{FUSION}(MW) = \alpha \bullet n_d \bullet W_{fast}$ (MJ) where $\alpha = 7.3 \bullet 10^{-21} m^3/s$.

In **conclusion** , using the JET advanced ICRH phasing and matching techniques with feedback control system on frequency, stubs and plasma position and antennas with Be-screens, we have developed and exploited new regimes of operation such as pellet enhanced phase (PEP), H-modes, PEP + H mode, monster sawteeth, synergism in current drive with LHCD, minority current drive effect on sawteeth etc. The evidence of majority ion heating ($T_{i0} \geq T_{e0}$) at high minority concentration gives confidence to propose the high D-minority ($\cong$ 30%) in tritium plasma ICRH driven scenario which is expected to minimze the power required to reach ignition.

ACKNOWLEDGEMENTS.

We wish to thank G. Bosia, A. Sibley, T. Wade and the ICRH and LHCD plant teams, P. Lomas and the tokamak operation team and, A. Edwards and those operating the diagnostics used in the experiments reported in this paper. We also thank C.D. Challis, C. Gowers, P. Kupschus, D. Stork and B.J.D. Tubbing for their help with certain experiments.

REFERENCES.

[1] WADE T. et al (1991) Proc. 14 Symp. Fusion Engg, San Diego, to be published.
[2] KAYE A.S. et al (1987) Fusion Technology, 2, 203.
[3] WALKER, C.I., Proc. 15th Symp. Fusion Techno, Utrecht, Holland, (1988) 444.
[4] BOSIA, G., et al (1989) Fusion Eng. Design 11, 459.
[5] BOSIA, G., et al (1991) publication under preparation.
[6] REBUT, P.H. et al, (1988) IAEA Conf., Nice, France, CN-50/D-4-1.
[7] GOLDSTON, R. (1984) , Plasma Phys. Controlled Fusion 26, 87
[8] BHATNAGAR V.P. et al, (1991) Proc 18 EPS Plasma Phys Conf, Berlin, I, 369.
[9] JACQUINOT, J. et al, (1991) Plasma Phys and Contr. Fusion (to be published).
[10] D'IPPOLITO, D. et al, Sherwood Theory Conf., Seattle, Washington, 1991.
[11] SCHMIDT, G. et al, (1988) IAEA Conf., Nice, France, CN-50/A-4-1.
[12] BHATNAGAR, V.P. al (1989) Plasma Phys Contr. Fusion, 31, 2111.
[13] TUBBING, B.J.D. et al (1991) Nuclear Fusion, to be published.
[14] HUGON, M. et al (1991) submitted to Nuclear Fusion.
[15] BHATNAGAR, V.P. al (1989) Plasma Phys Contr. Fusion, 33, 99.
[16] JACQUINOT J. et al, (1988) Plasma Phys and Contr Fusion, 30, 1467.
[17] COTTRELL G.A. et al, (1989) Plasma Phys and Contr Fusion, 31, 1727.
[18] KOCH, R. et al (1990) IAEA Conf. Washington, paper CN-53/G-2-9.
[19] STIX, T.H., Nuclear Fusion, 15 (1975) 737.
[20] START D.F.H. et al,(1991) Proc IOP Plasma Phys Conf, Colchester, UK.
[21] GORMEZANO et al, (1991) Proc 18 EPS Plasma Phys Conf, Berlin, III, 393.
[22] BRUSATI, M. et al, (1991) these proceedings.
[23] FROISSARD et al, (1991) Proc 18 EPS Plasma Phys Conf, Berlin, III, 389.
[24] COX, M. and D.F.H. START (1987) Int Conf Plasma Phys, Kiev, 1, 232.
[25] JACQUINOT, J. et al (1991) JET Joint Undertaking, Report JET-P(91)07.
[26] KUPSCHUS, P. et al, (1991) Proc 18 EPS Conf Plasma Phys, Berlin, I, 1.

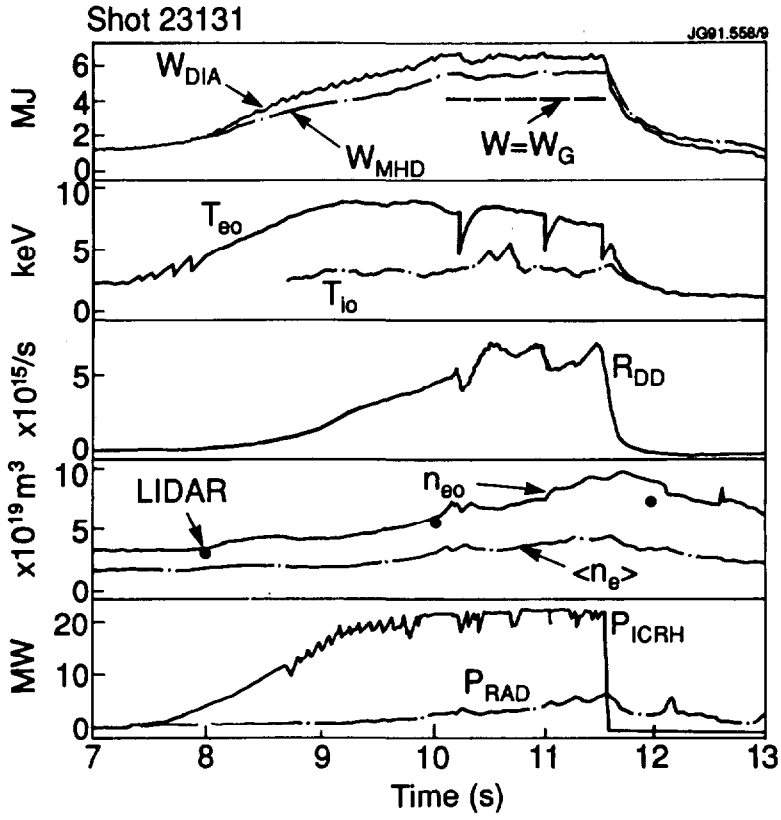

FIG. 1. Time traces of a ≅ 22 MW ICRF heated discharge in (H)-D plasma. Monster sawteeth are a characteristic of such discharges. W_G refers to Goldston L-mode prediction.

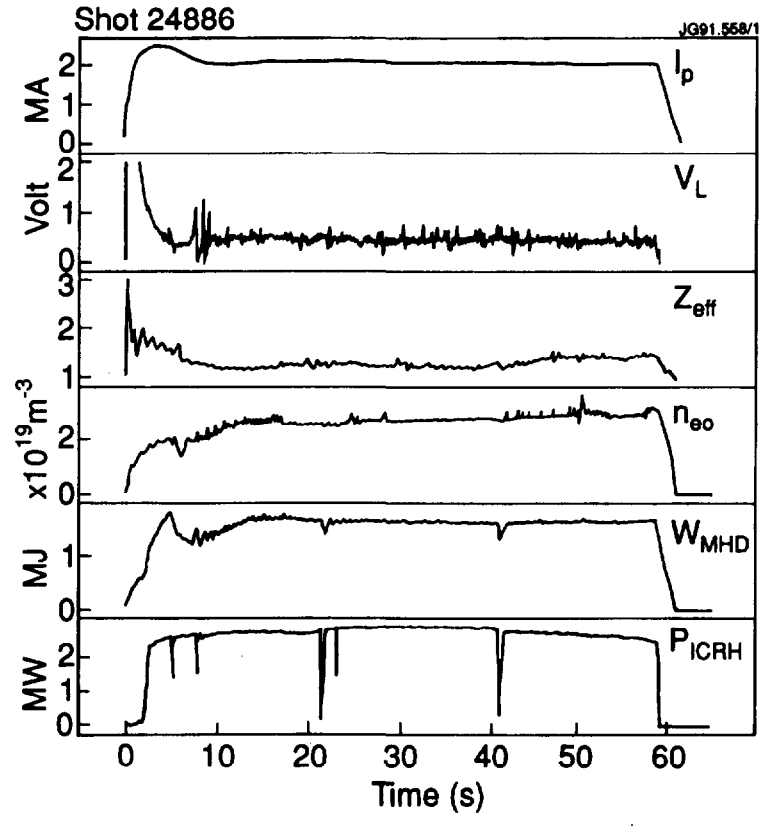

FIG. 2. Time evolution of a 60s long ICRH heated discharge. Electron heating due to ICRH increased the pulse length by 16 s. V_L = loop voltage, W_{MHD} = equilibrium stored energy.

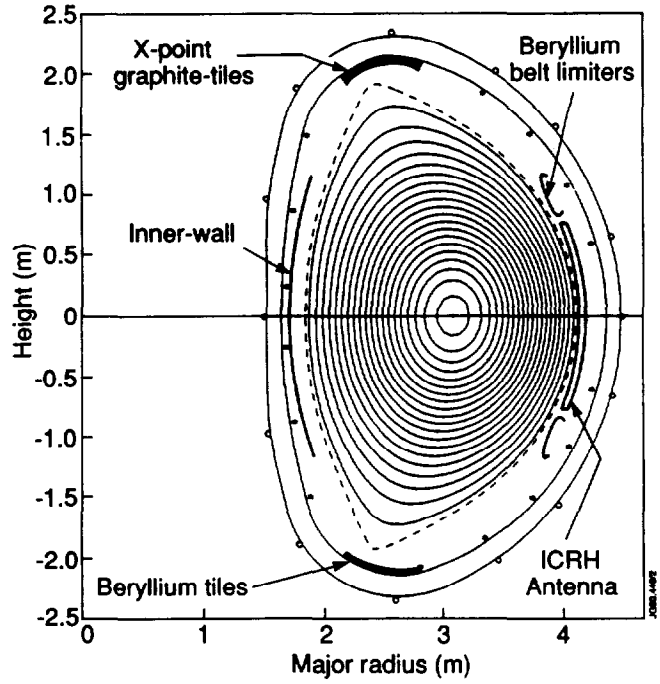

FIG. 3. Poloidal-flux contours from the IDENTC equilibrium code showing the double-null X-point configurationfor an ICRH H-mode plasma. In 1991 lower Be belt limiters have been replaced by graphite limiter tiles.

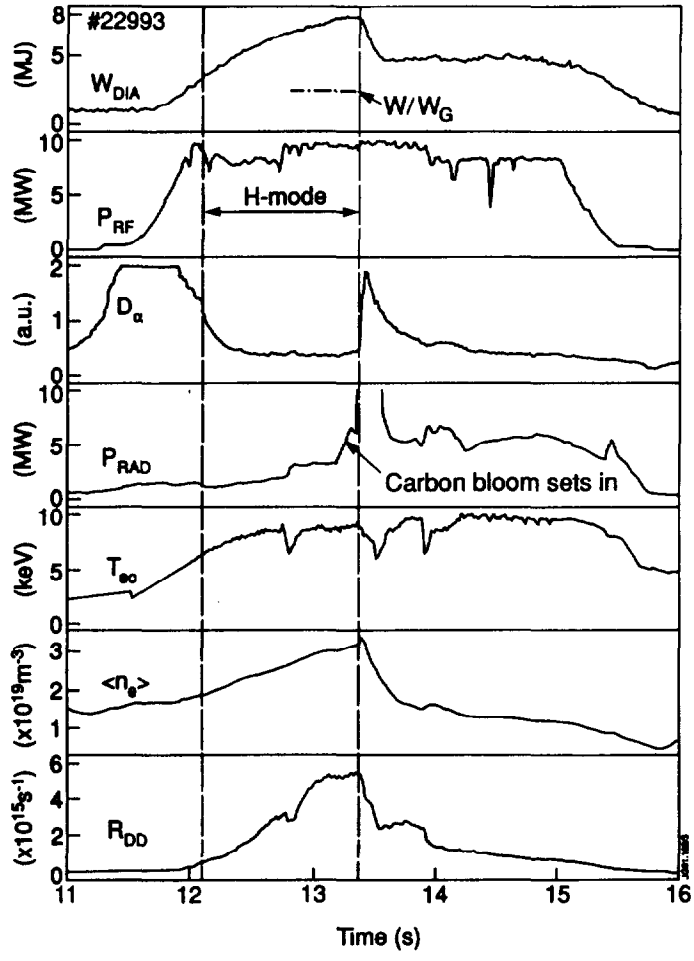

FIG. 4. Time traces of an H-mode discharge with ICRH alone using dipole antenna.

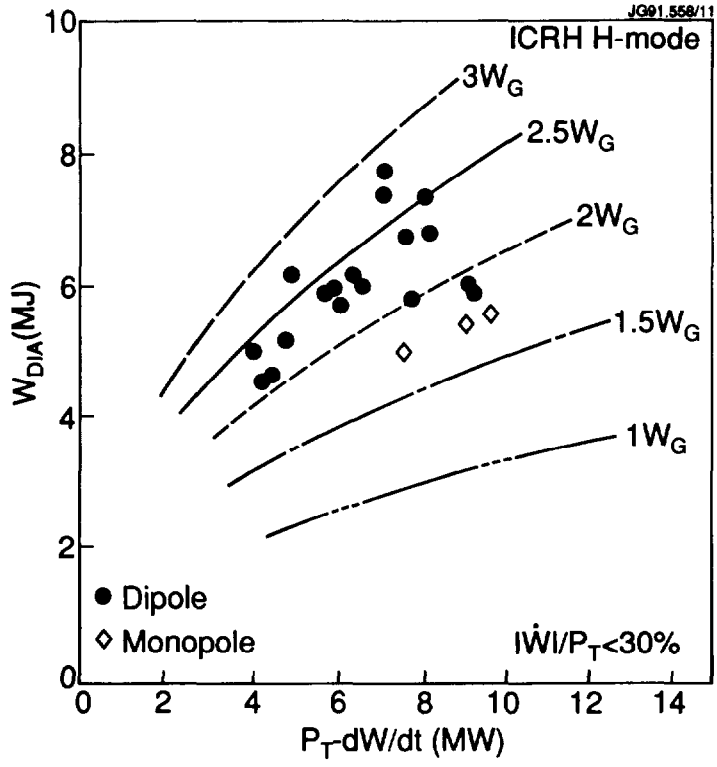

FIG. 5. Diamagnetic loop measured plasma stored-energy vs loss power in ICRH H-mode discharges with monopole and dipole phasing. W_G represents the Goldston L-mode prediction for such discharges.

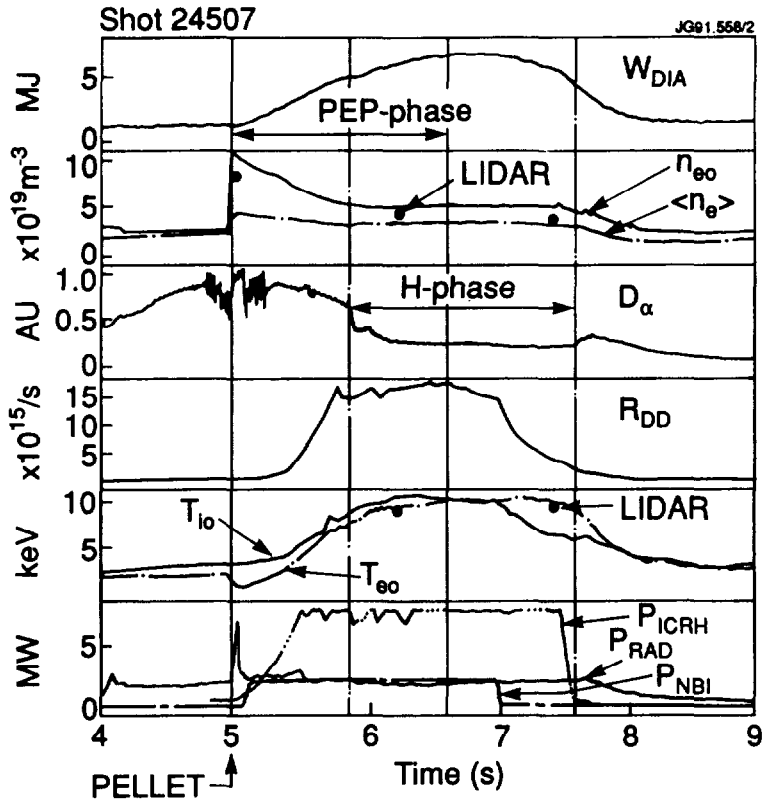

FIG. 6. Time traces of a Pellet Enhanced Phase (PEP) + H-mode discharge where the respective phases are indicated. The ECE T_{e0} data between 6.2-7.4s was unavailable and is joined by a straight line. LIDAR measured n_{e0} and T_{e0} are also shown. < ne > represents the volume average density. See remark in Fig. 8.

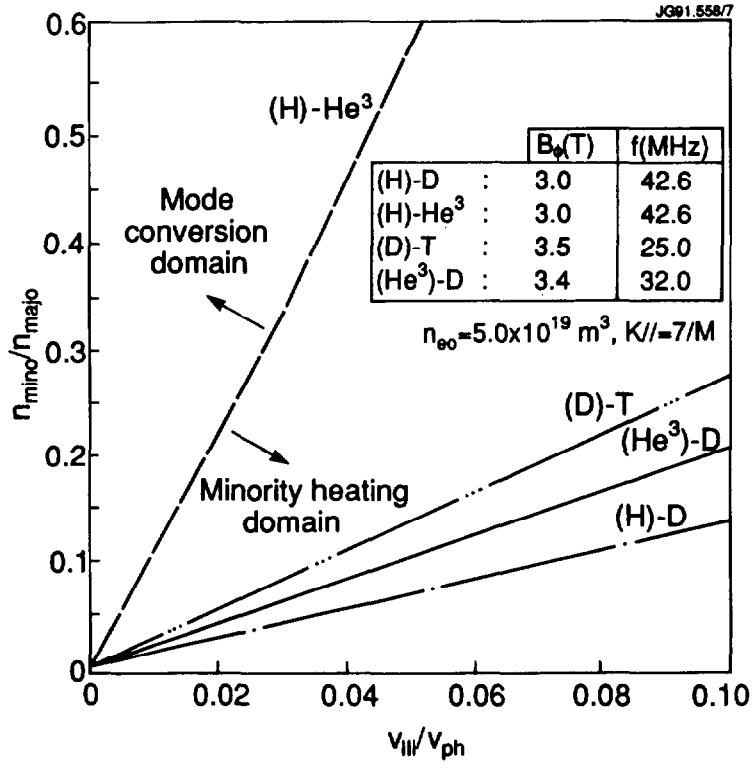

FIG. 7. A theoretical prediction for the occurence of mode conversion where minority to majority concentration is plotted vs minority ion $v_{//}/v_{ph}$ for several JET scenarios where v_{ph} is $\omega/k_{//}$. Minority heating occurs below the curves as shown. For different curves, density is constant.

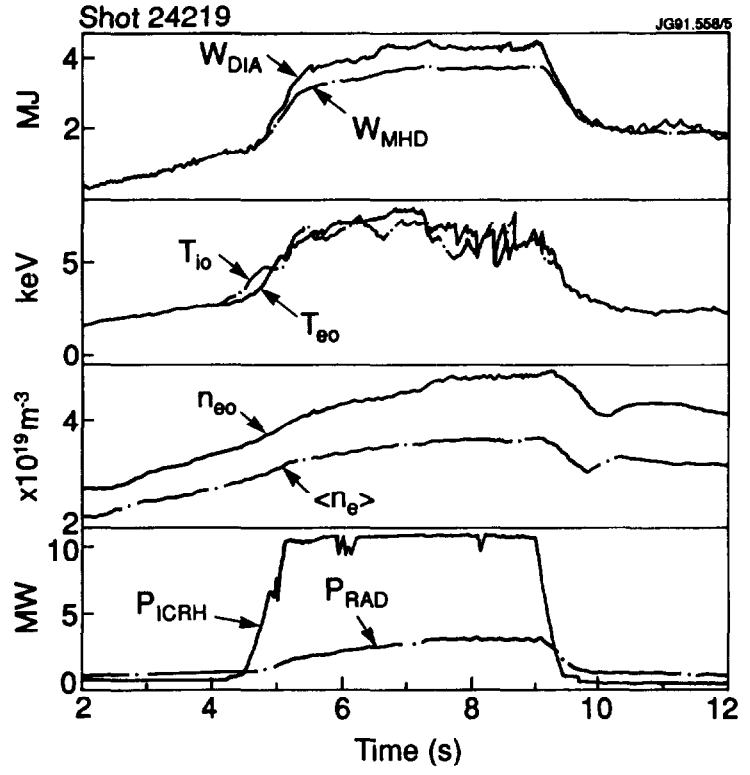

FIG. 8. Time traces of a high concentration minority heating in a (H)-He3 plasma where $n_H/n_e \cong 0.3$. Remark: T_{i0} was measured by Doppler broadening of Ni^{27}-line. T_{i0} is generally 30% higher than shown in this paper when corrections due to central burn out of He-like Ni-line and n_e profile effects are taken into account.

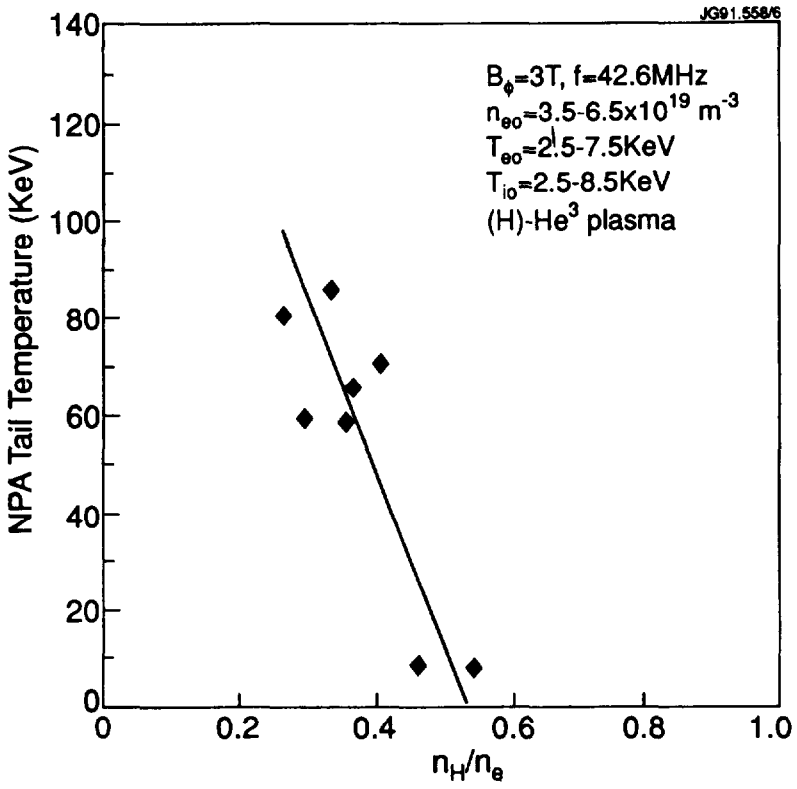

FIG. 9. Neutral particle analyser measured minority tail tamperature plotted vs minority concentration in the high minority (H)-He3 scenario. For the lowest two points, minority/majority was strongly inverted.

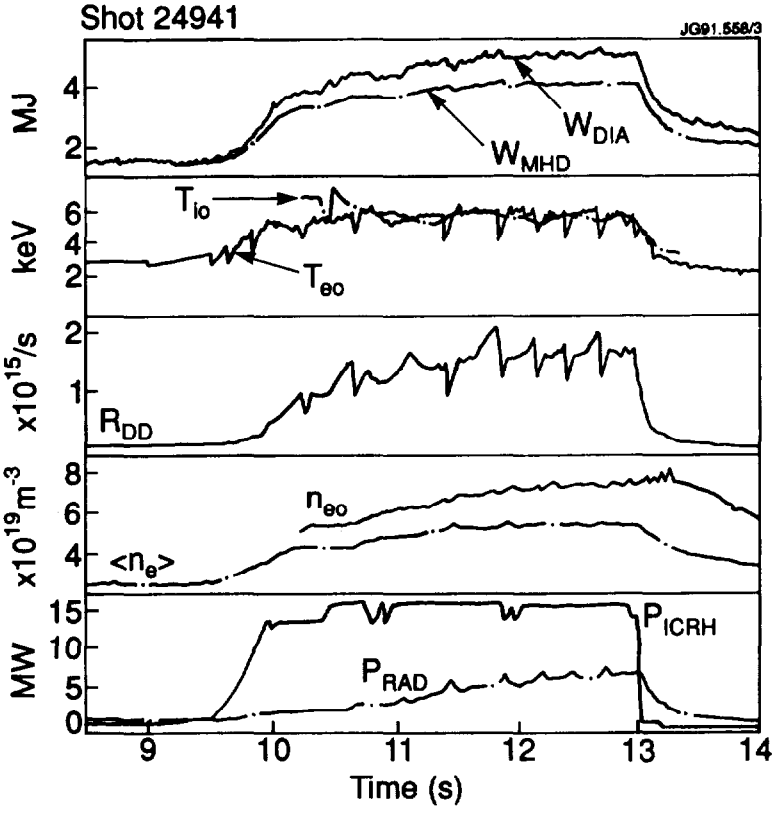

FIG. 10. Time traces of a two-minority (H and He3) ICRF heating experiment. $P_H = 9MW$ and $P_{He3} = 6.6MW$. $T_{i0} \geq T_{e0}$. See remark in Fig. 8 on T_{i0} which is an underestimate. In this case, no monster sawtooth was obtained.

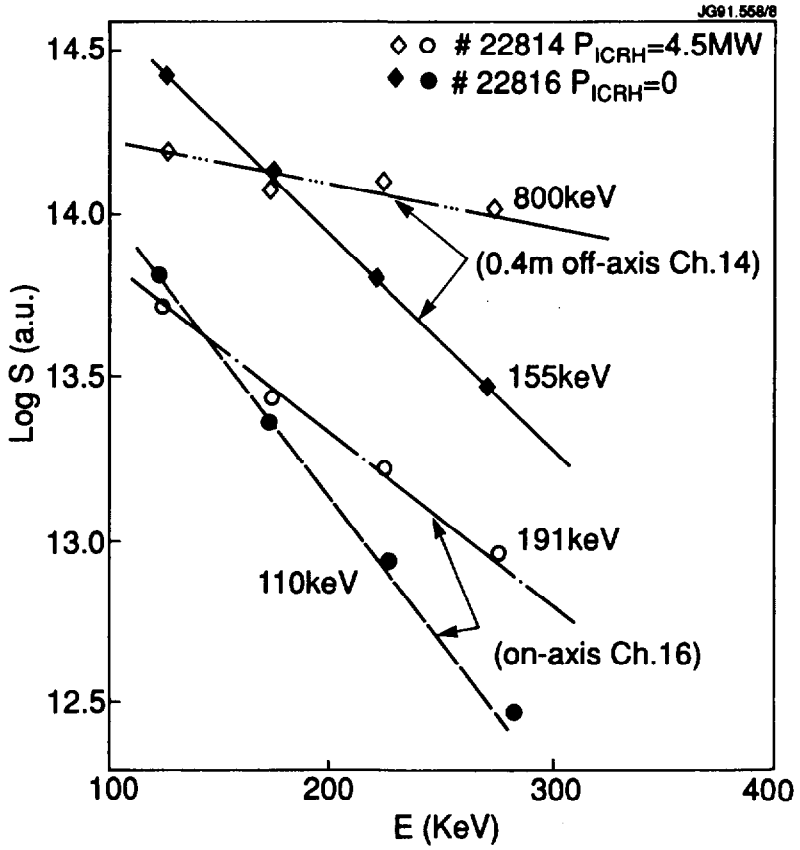

FIG. 11. Fast electron Bremstrahlung (FEB) measured photon distribution vs photon energy measured perpendicular to B_ϕ. The LHCD power = 1.2 MW. The synergistic effect is more pronounced off-axis in the densest region of fast electrons.

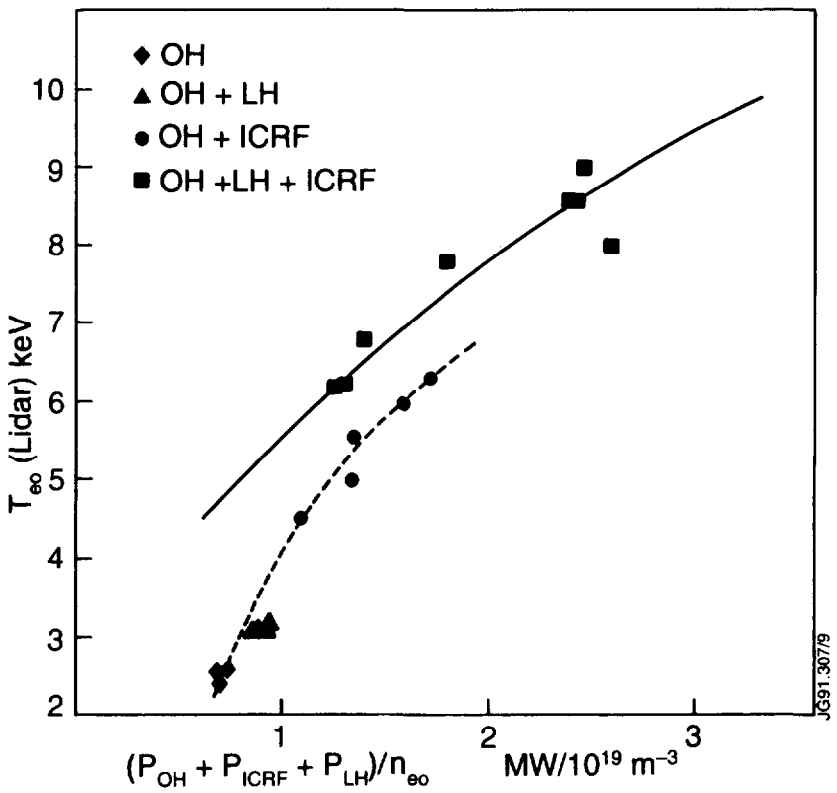

FIG. 12. T_{e0} from Thomson scattering diagnostic vs the total input power showing the synergistic effect on T_{e0}.

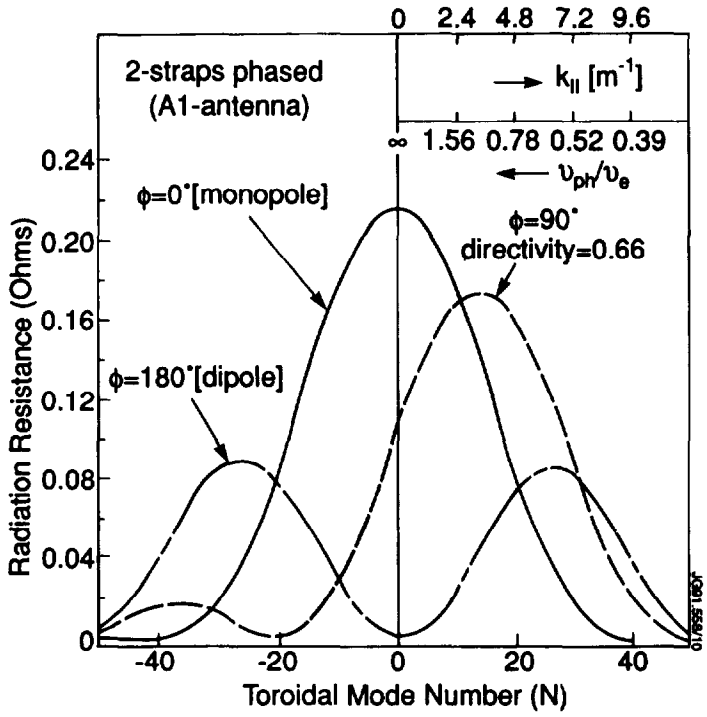

FIG. 13. Radiated power spectrum vs toroidal mode number of a dipole, monopole and 90°-phased two-straps of a JET A1-antenna with Fast-wave propgating into a typical JET plasma.

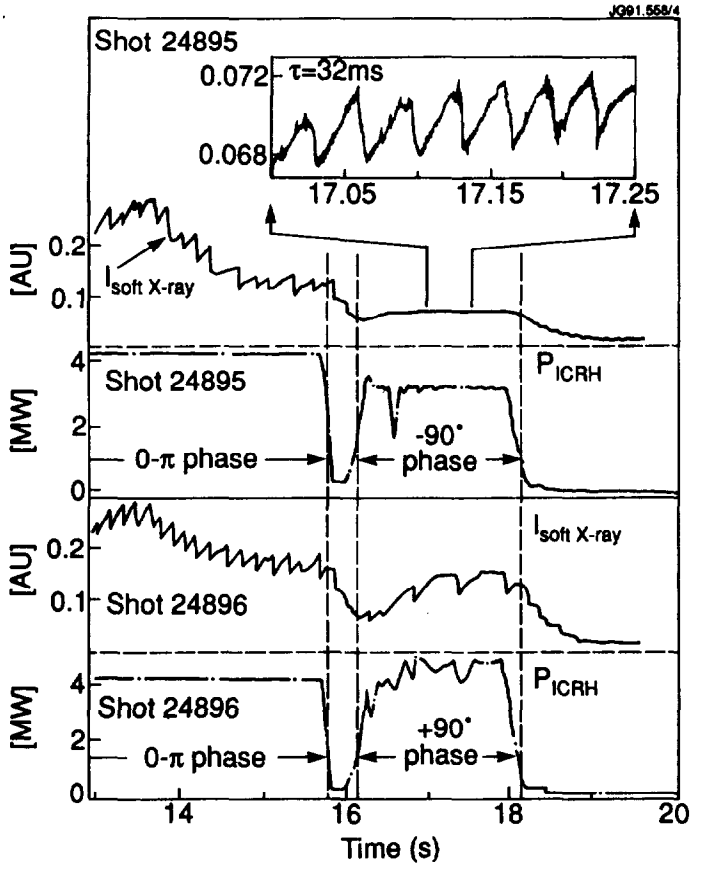

FIG. 14. Differnce in the sawtooth behaviour as measured by soft X-ray under minority heating near q = 1 on the high field side with a dipole, +90° and -90° phased antennas. Inset shows a blow up of the frequent ($\tau \cong 30ms$) and small amplitude (5%) sawteeth observed with -90° phasing.

Appendix I

THE JET TEAM

JET Joint Undertaking, Abingdon, Oxon, OX14 3EA, U.K.

J.M. Adams[1], H. Altmann, A. Andersen[14], P. Andrew[18], M. Angelone[29], S.A. Arshad, W. Bailey, P. Ballantyne, B. Balet, P. Barabaschi, R. Barnsley[2], M. Baronian, D.V. Bartlett, A.C. Bell, I. Benfatto[5], G. Benali, H. Bergsaker[11], P. Bertoldi, E. Bertolini, V. Bhatnagar, A.J. Bickley, H. Bindslev[14], T. Bonicelli, S.J. Booth, G. Bosia, M. Botman, D. Boucher, P. Boucquey, P. Breger, H. Brelen, H. Brinkschulte, T. Brown, M. Brusati, T. Budd, M. Bures, T. Businaro, P. Butcher, H. Buttgereit, C. Caldwell-Nichols, D.J. Campbell, P. Card, G. Celentano, C.D. Challis, A.V.Chankin[23], D. Chiron, J. Christiansen, C. Christodoulopoulos, P. Chuilon, R. Claesen, S. Clement, E. Clipsham, J.P. Coad, M. Comiskey[4], S. Conroy, M. Cooke, S. Cooper, J.G. Cordey, W. Core, G. Corrigan, S. Corti, A.E. Costley, G. Cottrell, M. Cox[7], P. Cripwell, H. de Blank[15], H. de Esch, L. de Kock, E. Deksnis, G.B. Denne-Hinnov, G. Deschamps, K.J. Dietz, S.L. Dmitrenko, J. Dobbing, N. Dolgetta, S.E. Dorling, P.G. Doyle, D.F. Düchs, H. Duquenoy, A. Edwards, J. Ehrenberg, A. Ekedahl, T. Elevant[11], S.K. Erents[7], L.G. Eriksson, H. Fajemirokun[12], H. Falter, D. Flory, J. Freiling[15], C. Froger, P. Froissard, K. Fullard, M. Gadeberg, A. Galetsas, D. Gambier, M. Garribba, P. Gaze, R. Giannella, A. Gibson, R.D. Gill, A. Girard, A. Gondhalekar, C. Gormezano, N.A. Gottardi, C. Gowers, B.J. Green, R. Haange, G Haas, A. Haigh, G. Hammett[6], C.J. Hancock, P.J. Harbour, N.C. Hawkes[7], P. Haynes[7], J.L. Hemmerich, T. Hender[7], F.B. Herzog, R.F. Herzog, J. Hoekzema, J. How, M. Huart, L Hughes, T.P. Hughes[4], M. Hugon, M. Huguet, A. Hwang[7], B. Ingram, M. Irving, J. Jacquinot, H. Jaeckel, J.F. Jaeger, G. Janeschitz[13], S. Jankowicz[22], O.N. Jarvis, F. Jensen, E.M. Jones, L.P.D.F. Jones, T.T.C. Jones, J-F. Junger, E. Junique, A. Kaye, B.E. Keen, M. Keilhacker, G.J. Kelly, W. Kerner, R. Konig, A. Konstantellos, M. Kovanen[20], G. Kramer[15], P. Kupschus, R. Lässer, J.R. Last, B. Laundy, L. Lauro-Taroni, K. Lawson[7], M. Lennholm, A. Loarte, R. Lobel, P. Lomas, M. Loughlin, C. Lowry, B. Macklin, G. Maddison[7], G. Magyar, W. Mandl[13], V. Marchese, F. Marcus, J. Mart, E. Martin, R. Martin-Solis[8], P. Massmann, G. McCracken[7], P. Meriguet, P. Miele, S.F. Mills, P. Millward, R. Mohanti[17], P.L. Mondino, A. Montvai[3], S. Moriyama[28], P. Morgan, H. Morsi, G. Murphy, M. Mynarends, R. Myrnäs[16], C. Nardone, F. Nave[21], G. Newbert, M. Newman, P. Nielsen, P. Noll, W. Obert, D. O'Brien, J. O'Rourke, R. Ostrom, M. Ottaviani, M. Pain, F. Paoletti, S. Papastergiou, D. Pasini, A. Peacock, N. Peacock[7], D. Pearson[12], R. Pepe de Silva, G. Perinic, C. Perry, M. Pick, R. Pitts[7], J. Plancoulaine, J-P. Poffé, F. Porcelli, L. Porte[19], R. Prentice, S. Puppin, S. Putvinsko[23], G. Radford[9], T. Raimondi, M.C. Ramos de Andrade, P-H. Rebut, R. Reichle, E. Righi, F. Rimini, D. Robinson[7], A. Rolfe, R.T. Ross, L. Rossi, R. Russ, P. Rutter, H.C. Sack, G. Sadler, G. Saibene, J.L. Salanave, G. Sanazzaro, A. Santagiustina, R. Sartori, C. Sborchia, P. Schild, M. Schmid, G. Schmidt[6], B. Schunke, S.M. Scott, A. Sibley, R. Simonini, A.C.C. Sips, P. Smeulders, R. Stankiewicz[27], M. Stamp, P. Stangeby[18], D.F. Start, C.A. Steed, D. Stork, P.E. Stott, T.E. Stringer, P. Stubberfield, D. Summers, H. Summers[19], L. Svensson, J.A. Tagle[21], A. Tanga, A. Taroni, A. Tesini, P.R. Thomas, E. Thompson, K. Thomsen, J.M. Todd, P. Trevalion, B. Tubbing, F. Tibone, E. Usselmann, H. van der Beken, G. Vlases, M. von Hellermann, T. Wade, C. Walker, R. Walton[6], D. Ward, M.L. Watkins, M.J. Watson, S. Weber[10], J. Wesson, T.J. Wijnands, J. Wilks, D. Wilson, T. Winkel, R. Wolf, B. Wolle[24], D. Wong, C. Woodward, Y. Wu[25], M. Wykes, I.D. Young, L. Zannelli, Y. Zhu[26], W. Zwingmann.

PERMANENT ADDRESSES

1. UKAEA, Harwell, Didcot, Oxon, UK.
2. University of Leicester, Leicester, UK.
3. Central Research Institute for Physics, Academy of Sciences, Budapest, Hungary.
4. University of Essex, Colchester, UK.
5. ENEA-CNR, Padova, Italy.
6. Princeton Plasma Physics Laboratory, New Jersey, USA.
7. UKAEA Culham Laboratory, Abingdon, Oxon, UK.
8. Universidad Complutense de Madrid, Spain.
9. Institute of Mathematics, University of Oxford, UK.
10. Freien Universität, Berlin, F.R.G.
11. Swedish Energy Research Commission, S-10072 Stockholm, Sweden.
12. Imperial College of Science and Technology, University of London, UK.
13. Max Planck Institut für Plasmaphysik, Garching bei München, FRG.
14. Risø National Laboratory, Denmark.
15. FOM Instituut voor Plasmafysica, 3430 Be Nieuwegein, The Netherlands.
16. University of Lund, Sweden.
17. North Carolina State University, Raleigh, NC, USA
18. Institute for Aerospace Studies, University of Toronto, Downsview, Ontario, Canada.
19. University of Strathclyde, 107 Rottenrow, Glasgow, UK.
20. Nuclear Engineering Laboratory, Lapeenranta University, Finland.
21. CIEMAT, Madrid, Spain.
22. Institute for Nuclear Studies, Otwock-Swierk, Poland.
23. Kurchatov Institute of Atomic Energy, Moscow, USSR
24. University of Heidelberg, Heidelberg, FRG.
25. Institute for Mechanics, Academia Sinica, Beijing, P.R. China.
26. Southwestern University of Physics, Leshan, P.R. China.
27. RCC Cyfronet, Otwock Swierk, Poland.
28. JAERI, Naka Fusion Research Establishment, Ibaraki, Japan.
29. ENEA, Frascati, Italy.

At 1st June 1991